Supplementary information to accompany the paper entitled:

The pollen record of marine core MD03-2607 offshore Kangaroo Island spanning the last 125 kyears; implications for vegetation changes across the Murray-Darling Basin

Patrick De Deckker[a], Sander van der Kaars[b,c], Simon Haberle[d,e], Quan Hua[f], Jan-Berend W. Stuut[g]

[a]Research School of Earth Sciences, The Australian National University, Canberra ACT2601; [b]School of Earth, Atmosphere and Environment, Monash University, Clayton VIC 3800; [c]Department of Earth Sciences, Vrije Universiteit Amsterdam, 1081 HV Amsterdam, The Netherlands; [d]School of Culture, History and Language, The Australian National University, Canberra ACT 2601; [e]ARC Centre of Excellence for Australian Biodiversity and Heritage, The Australian National University, Canberra ACT 2601, [f]Australian Nuclear Science and Technology Organisation, Lucas Heights, NSW 2234, Australia; [g]NIOZ - Royal Netherlands Institute for Sea Research, and Utrecht University, 1797 SZ Den Hoorn, Texel, The Netherlands.

1.Description of core MD03-2607

Calypso core MD03-2607 was taken on February 21, 2003 with the RV *Marion Dufresne* during the AUSCAN campaign (Hill and De Deckker, 2004) on a flat platform east of Sprigg Canyon (Suppl. Fig. 1) southeast of Kangaroo Island. Its location is 36° 57.64' S, 137°E 24.39' and in 865m water depth. The core is 32.95 m long, with the upper 14.7 m (of interest here) consisting of massively bedded fine to very fine (foraminiferal) sands with minor colour variation from darker to paler olive grey. In this upper section of the core occasional zones of irregular or wavy cm-scale darker and lighter layers occur. Below 14.7m the sediments are finer textured.

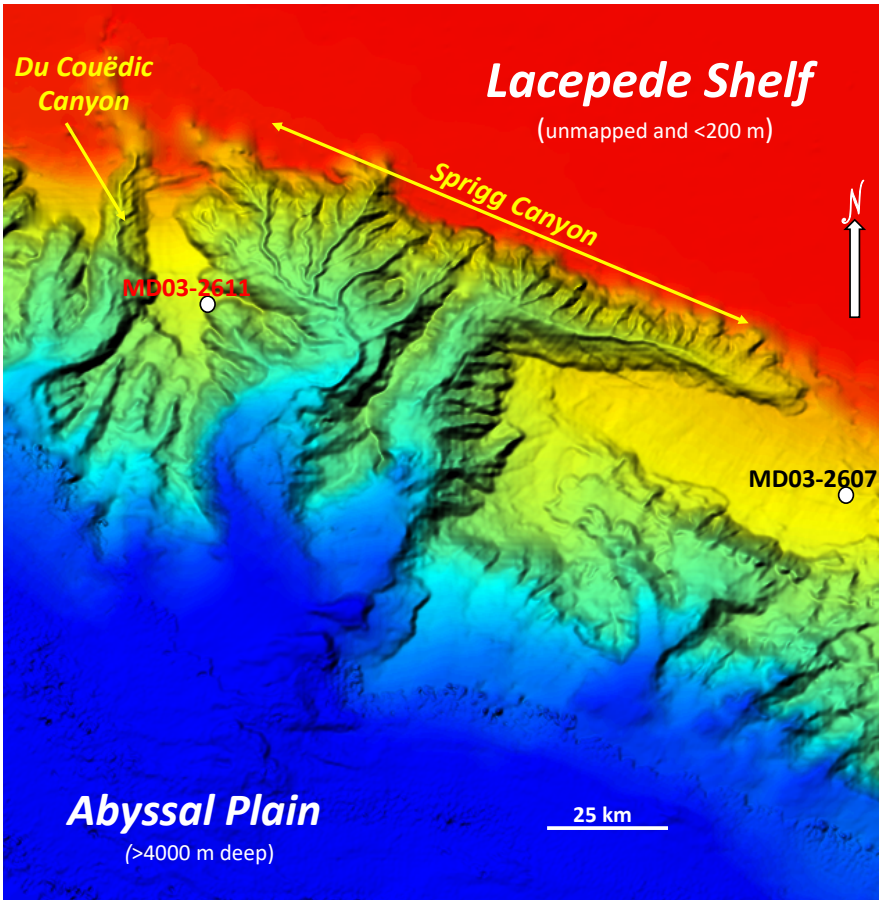

Supplementary figure 1. Tilted 3-D image showing a close up of the Sprigg Canyon and the adjacent du Couëdic Canyon located offshore the Lacepede Shelf (shown in red). The location of the two cores discussed in this paper is shown. Note that empty/hollow meanders are clearly visible in both canyons, suggesting that they are still active today. Image provided by Sharon Glasgow.

2.Photographic record of coring activities on board the *RV Marion Dufresne*

Supplementary figure 2. Photographs taken on the *RV Marion Dufresne* showing various activities linked to the retrieval of core MD03-2607. **A:** The 40 m long metal barrel of the Calypso corer is hanging over the side of the ship and is attached to the 800 kg lead weight (painted yellow) before being brought back on the side deck; **B:** The metal barrel inside which core MD03-2607 made of PVC is in the process of being extracted. Note the grey mud on the side of the barrel shows the extent of penetration into the sea floor. Other metal barrels lie on the side deck, ready for the next coring operation; **C:** a large portion of the PVC pipe has already been extracted from the metal barrel and lies on small supports along the front of the ship that is ~120 m long; **D:** people are in the process of labelling the PVC pipe that is to be cut into 1.5 m sections. Eventually each section will be split open lengthwise on board and various measurements will be made soon afterwards, such as sediment logging, colourimetry, magnetic measurements and small samples extraction for microscopic examination. For additional information and photographs, refer to the report made by Hill and De Deckker (2004).

3.Core chronology

The figures below show the approach taken to obtain a sound chronology for core MD03-2607.

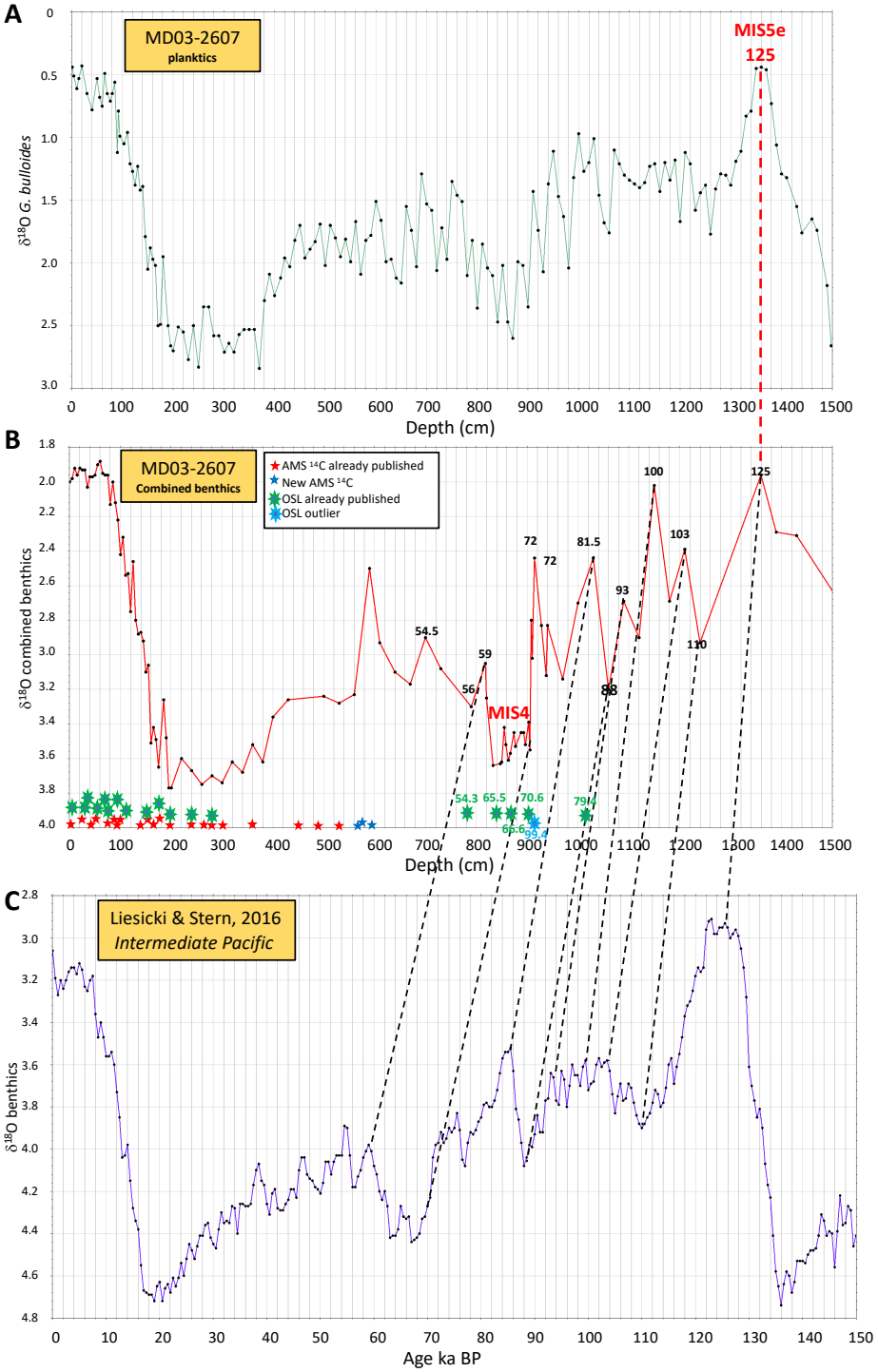

Supplementary figure 3. Correlation between various $\delta^{18}O$ curves that were used to provide tie points for dating older parts of core MD03-2607. **A**: The $\delta^{18}O$ of the planktic foraminifera *G. bulloides* from core MD03-2607 help confirm the culmination of MIS5e at 125 ka; **B:** the $\delta^{18}O$ record of a combination of benthic foraminifera obtained from Lopes dos Santos et al. (2013a) and De Deckker et al. (2019). In addition, all the position of all the AMS radiocarbon dates taken from the core are shown as red stars (taken from Lopes dos Santos et al. (2012), with three new ones shown as blue stars. In addition, the position on the core where OSL samples were taken are shown as green stars (taken from Lopes dos Santos et al. (2012) with the ages for the critical samples in the middle portion of the core shown with one outlier shown in pale blue (taken from De Deckker et al., 2019); **C:** the $\delta^{18}O$ of benthic foraminifera stack curve (Liesicki and Stern, 2016) for Intermediate Waters for the Pacific Ocean. The dotted lines link respective steps from Liesicki and Stern (2016) that show the tie points and respective ages used to provide ages. All these ages were then used to model the ages for the lower part of the core as shown in Supp. Fig. 4.

4.Age model

The figure below shows the age model calculated for the entirety of the core.

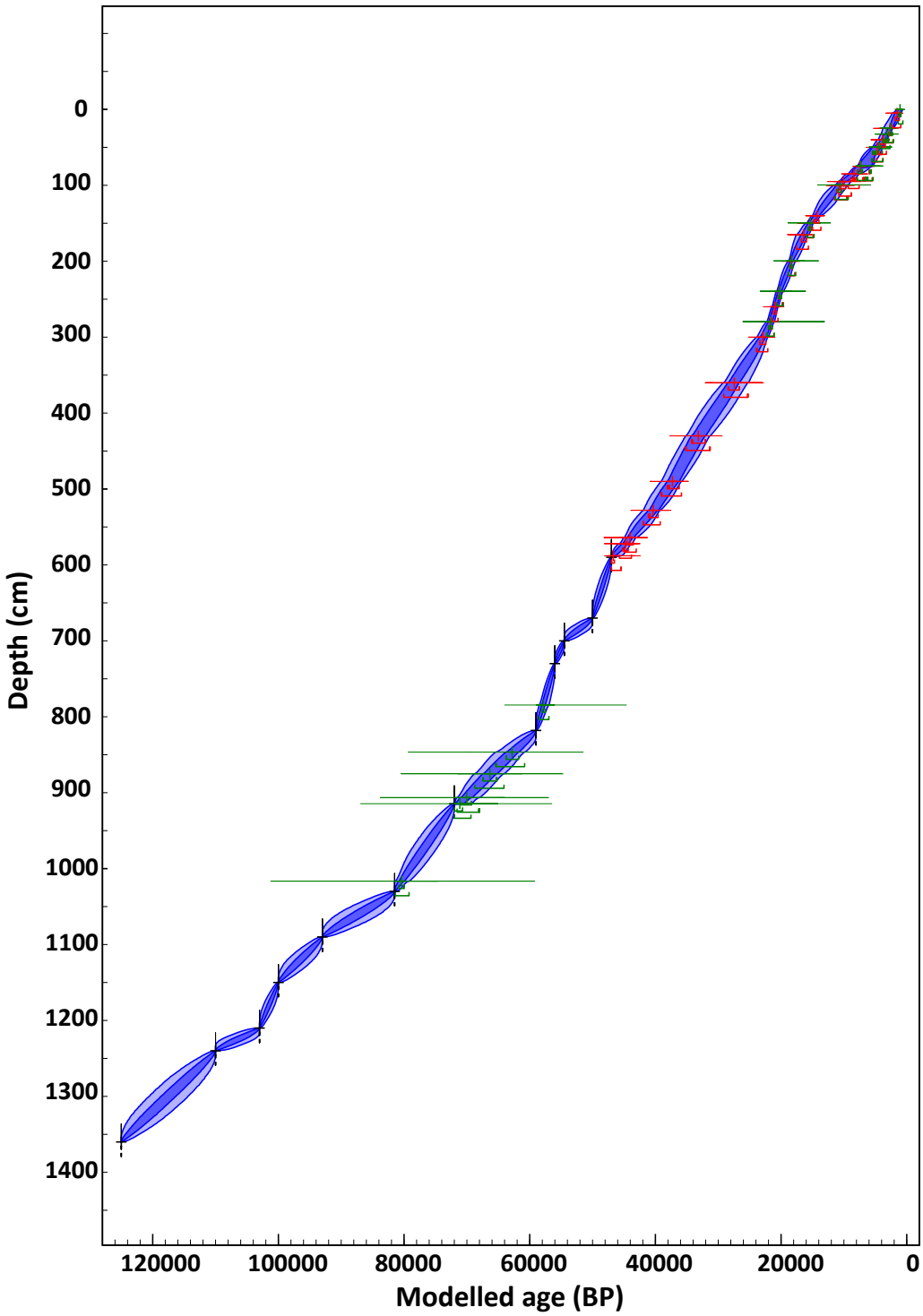

Supplementary figure 4. Age-depth model for core MD03-2607 using Bayesian OxCal P sequence (deposition sequence) with variable deposition rate (*k*). A general outlier analysis (prior probability = 0.05). The SHCal20 (Hogg et al., 2020) calibration curve was used for age calibration of the ^{14}C dates, which were corrected for radiocarbon marine reservoir ages. The OSL and ^{14}C dates are shown in green and red, respectively. Meanwhile, Meanwhile, tie points position linked to the Liesicki and Stern (2016) curve for the Central Water Mass in the western Pacific Ocean shown in Suppl. Fig. 3 appear in black. The list of dates and tie points is provided in Suppl. Table 2.

5.Colour reflectance

Colour reflectance of the entire core was obtained following the technique applied by Lourens (2004) to deep-sea cores in the Mediterranean Sea. The measurements, carried out on the ship soon after the opening of the cores, clearly support this observation. A Minolta CM-508 spectrophotometer was used. Measurements were made every cm for the upper 10.5 m of the core and below that this was done at 2 cm intervals.

The profile obtained from the subtraction of the 700 and 400 nm wavelengths in the colour spectrum presented in Suppl. Fig. 5B, in combination with the 400 nm wavelength curve shown in Suppl. Fig. 5C, clearly points out to the similarity of the $\delta^{18}O$ of the planktic foraminifer *G. bulloides* presented in Suppl. Fig. 5A - as well the SST reconstructed curve seen in Supp. Fig. 5E – confirm that the core does not have any hiatus.

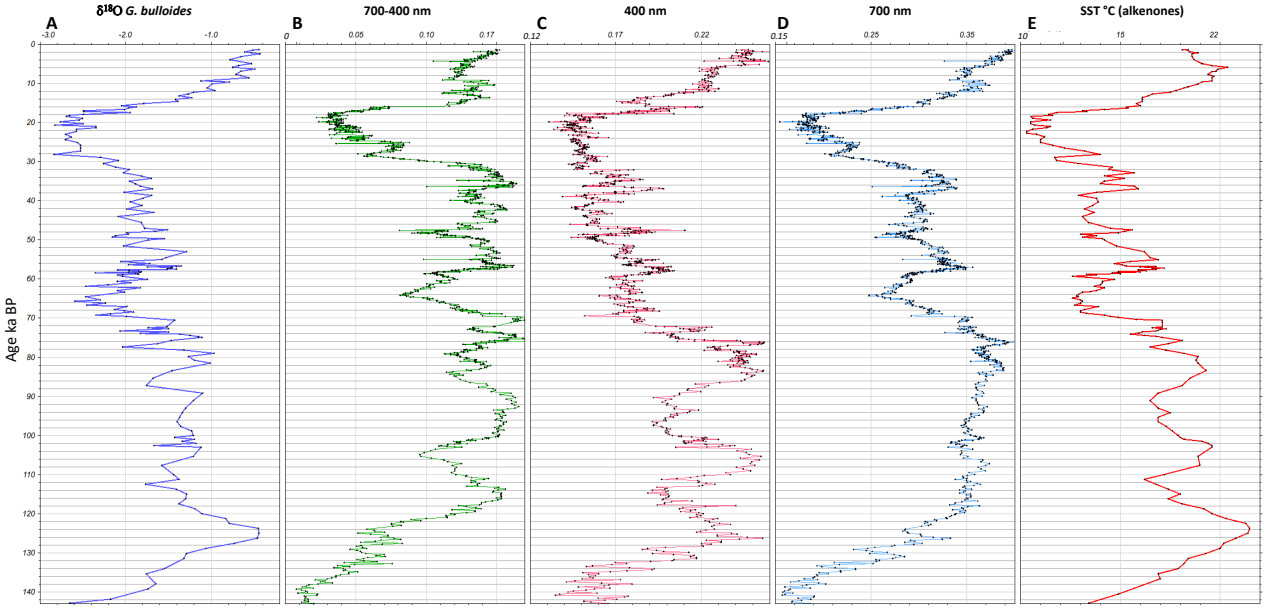

Supplementary figure 5. Correlation between various spectral colour reflectance spectra measured on core MD03-2607 soon after opening the core on the ship, against other proxies from the same core such as the $\delta^{18}O$ of foraminifera as an indicator of sea level changes, and sea-surface temperature obtained by alkenometry. **A:** The $\delta^{18}O$ of the planktic foraminifera *G. bulloides*; **B***:* Subtraction of the 700 and 400 nm wavelengths in the colour spectrum measured on the core; **C:** the 400 nm wavelength; **D:** the 700 nm wavelength; **E:** the SST record (Lopes dos Santos et al. (2013b) and De Deckker et al. (2019)). All these curves clearly show that there is no hiatus in the core, nor major turbidite.

6.Comparison between the pollen zonation and the marine isotope stages zonation

Suppl. Fig. 6 shows the zonations obtained for the pollen assemblages (PS1 to PZ11) using the arbitrary CONISS routine in TILIA (Grimm, 1987) and the Marine Isotope zonation following the standard nomenclature used by Liesicki and Stern (2016). Note that there is a good overall concordance between the two zonations with the exception of MIS3 that is subdivided into three pollen zones (PZ4 to PZ6). Additionally, the boundaries between MIS3/4 and MIS5d/MIS5e are slightly offset from the pollen zones but the differences are only of the order of 1 millennium or so and may well be caused by the absence of pollen counts for those horizons.

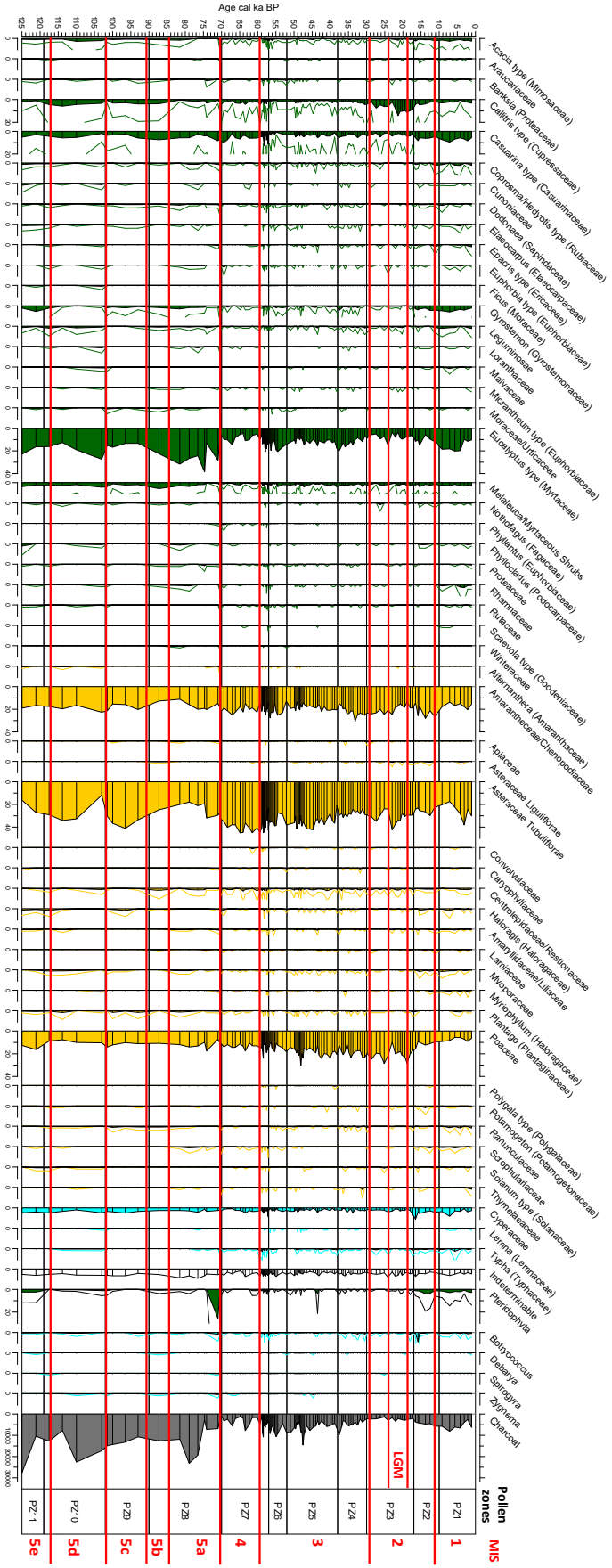

Supplementary figure 6. Complete pollen diagram of core MD03-2607 reproduced from figure 3 that shows the pollen zonation obtained by the CONISS routine in TILIA (Grimm, 1987) on which the Marine Isotope zonation following the standard nomenclature used by Liesicki and Stern (2016) is superimposed.

A diagram showing the output of the CONISS routine is provided in Supp. Fig. 7 and this routine places the main division in the diagram between pollen zones 2 and 3. This boundary is calculated on the basis of the greatest dissimilarity between zones using the taxa in this diagram only. The next division is indicated to occur between zones 3 and 4 and the following between zones 7 and 8. These divisions correspond fairly well with the MIS stages placed on the pollen diagram (see Supp. Fig. 6), especially for the latter two divisions (e.g.3-4 and 7-8).

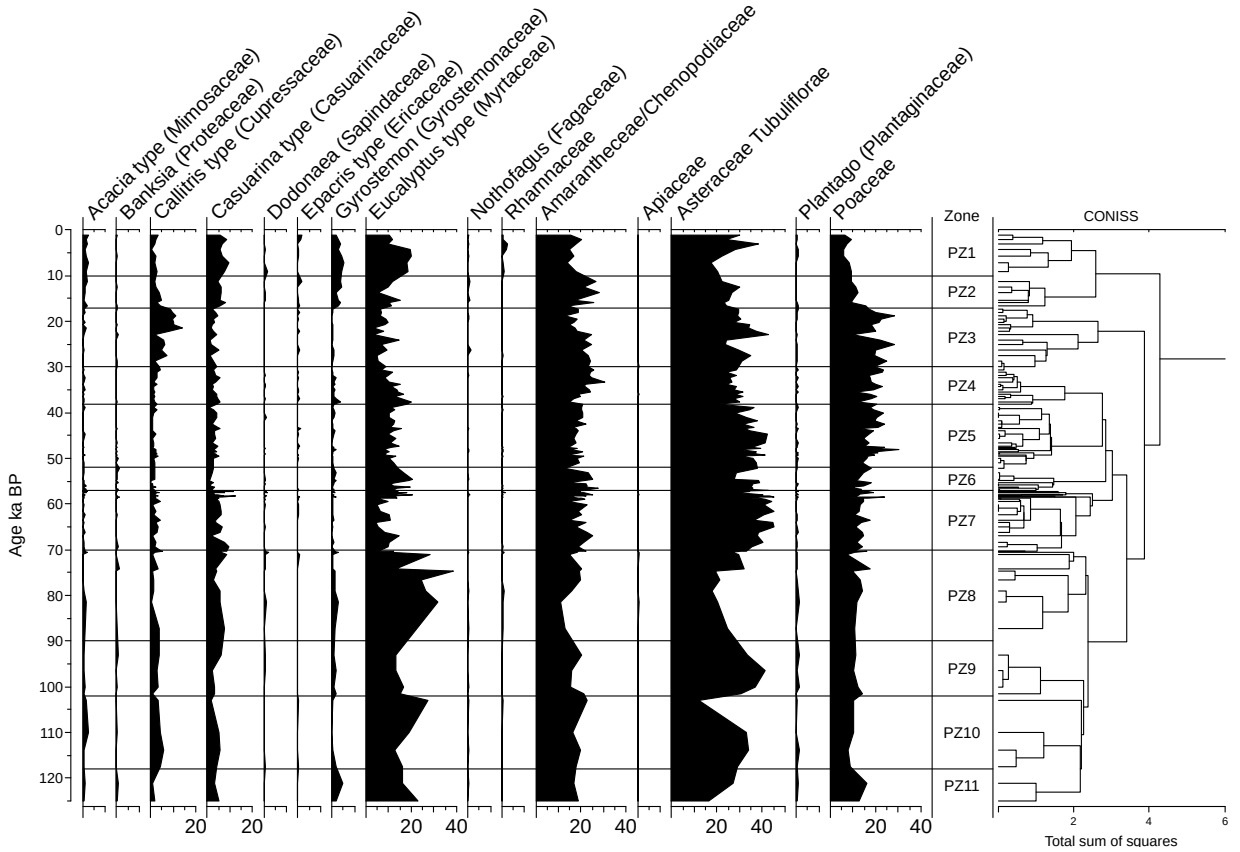

Supplementary figure 7. Routine diagram generated by the CONISS program that shows the hierarchy generated for the 120 pollen samples obtained from core 2607.

7.Clarifying the pollen signal in core 2607 using EMMAgeo

Pollen assemblages obtained from marine cores may have complex signatures because they may have been sourced from different geographic areas as well as from different environments within those areas. In order to attempt to clarify the different source areas, and potentially improve the interpretation of the pollen data from core 2607, the End Member Modelling program using EMMAgeo (Dietze and Dietze, 2019, Dietze et al., 2012) was undertaken in R (R Core Team, 2020). The pollen data were decomposed with the inversion algorithm for 'end-member modelling of compositional data' using EMMAgeo to construct a mixing model that expresses the observations as mixtures of a limited number of end-members. In the modelling stage, the 'mixing problem' is solved in two stages:

(1) The first modelling stage involves the estimation of optimal number (q) of end-members and weight loadings (l). This estimation is based on output from EMMAgeo that provides the mean/median coefficient of determination (r2) for combinations of q and l, and it represents the proportions of the variance explained for each variable (pollen taxon) that can be reproduced by the approximated data (Suppl. Fig. 8).

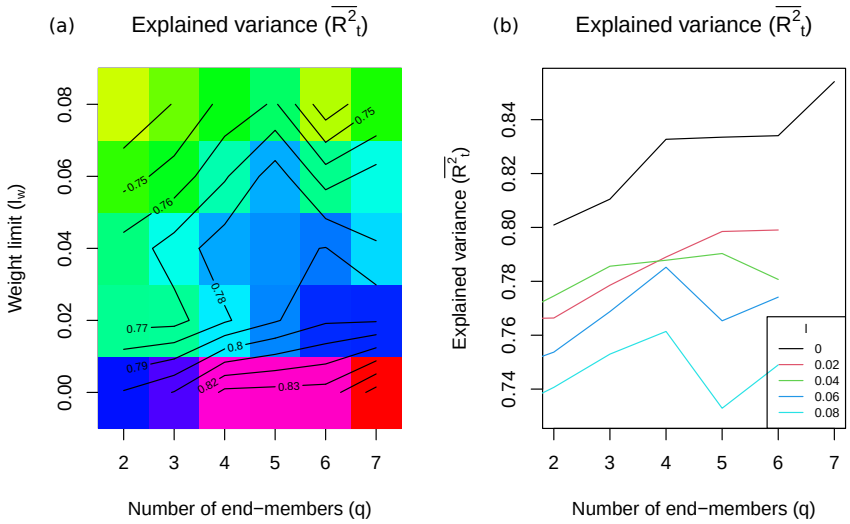

Supplementary figure 8. (a) Mean total Rt2 (explained variance) of all combinations of weight transformation limits (l) and number of end-members (q) and (b) of end-members (q) at selected weight transformation limits (l) from the output of EMMAgeo analysis of 16 selected pollen taxa from core 2607.

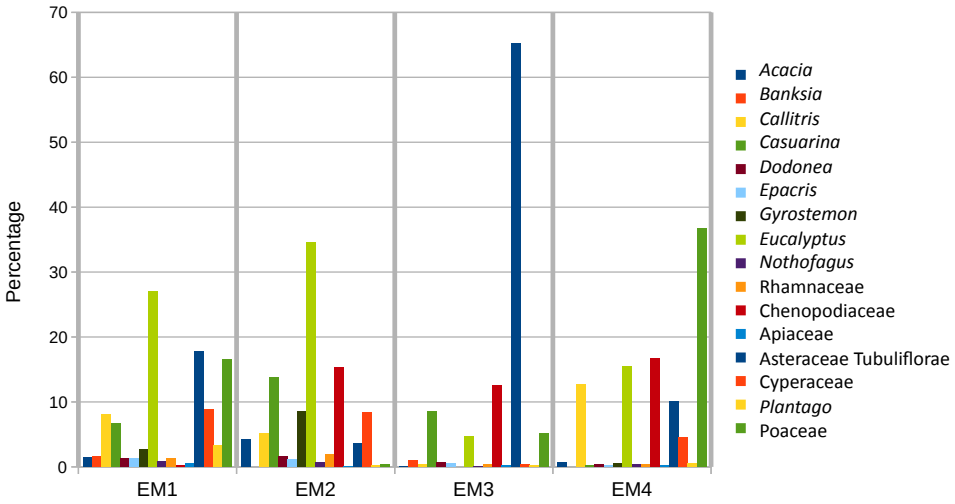

Supplementary figure 9. Histograms showing the composition of the 4 end-members resulting from modelling by EMMAgeo of 16 selected pollen taxa from core 2607.

The outcomes show that under different loadings the more robust models are generally achieved when using 4 end-members and that overall a weight loading of 0 produces more robust models;

(2) The second modelling stage involves estimation of the end-member compositions (disentangling and redistribution of pollen percentage data from 16 selected taxa from core 2607 over the 4 end-members) (Suppl. Figs. 9 and 10c), and subsequently, calculation of the proportional contribution of the end members at all core depths (Suppl. Fig. 10d). These end members – extreme, theoretical pollen assemblages - are representative of different types of vegetation and potential source areas.

We also used existing transfer functions from Cook and van der Kaars (2006) to reconstruct annual rainfall, summer rainfall and winter rainfall for each of the vegetation types, identified as EM1 to EM4. These are presented in Supplementary Table 1.

It is noteworthy that vegetation type EM4 (see Supp. Fig. 10) is by far the most arid of the four types. This type is sourced from the Murray sub-basin or, perhaps, it is the vegetation growing on the Lacepede Shelf when exposed during low sea level. We know form observations made at sea when surveying the Lacepede Shelf (P. De Deckker, personal observation during *Southern Surveyor* cruise SS02-06) that a large part of the entire shelf is currently covered with reworked red sand of dunal origin.

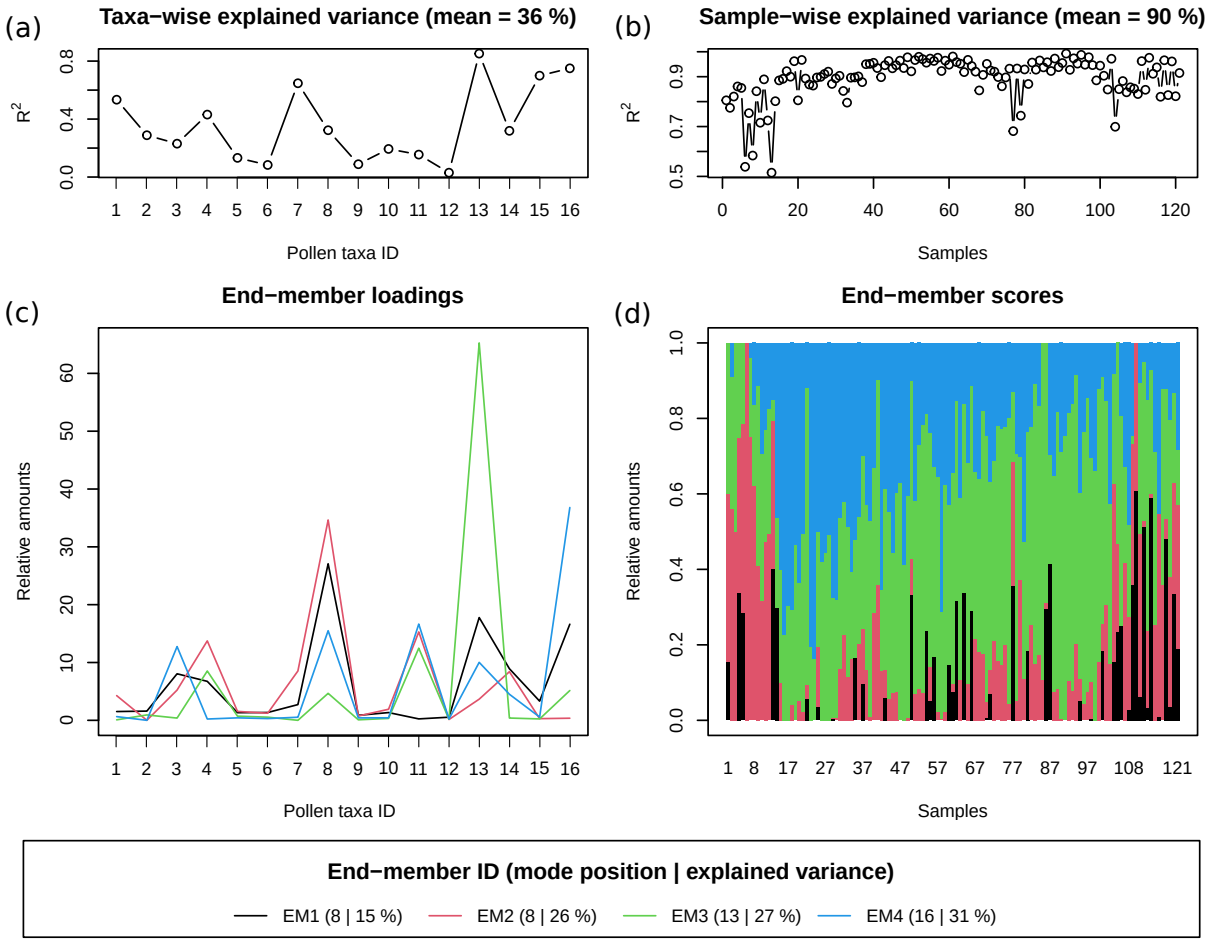

Supplementary figure 10. Graphical output of the EMMAgeo analysis using 16 selected pollen taxa with number of end-members set at 4 and weight transformation set at 0. (a, b) Measures of model performance (i.e. pollen taxa- and sample-wise R2) (squared Pearson correlation coefficients), (c) end-member loadings of individual pollen taxa and (d) end-member scores. The legend presents the main mode positions (pollen taxon ID) and explained variance of each end-member (%). Pollen taxa IDs are as follows. 1: *Acacia*, 2: B*anksia*, 3: *Callitris*, 4: *Casuarina*, 5: D*odonaea*, 6: *Epacris*, 7: G*yrostemon*, 8: *Eucalyptus*, 9: N*othofagus*, 10: Rhamnaceae, 11: Chenopodiaceae, 12: Apiaceae, 13: Asteraceae Tubuliflorae, 14: Cyperaceae, 15: P*lantago*, 16: Poaceae.

8.Comparison with other long pollen records from marine cores offshore Australia

Core E55-1 offshore Victoria

This core was taken at a water depth of 2,346 m to the west of the Otway Ranges (Fig. 1) and some 37 samples were analysed by Harle (1997) for the period that covered the last glacial/interglacial cycle. Unfortunately, the Holocene sequence was missing in that core due to a mud flow. By linking

the core to an oxygen isotope stratigraphy carried out by Passlow et al. (1997) it was possible to provide a chronology, which then enabled comparison of the pollen record with other sequences in Victoria that relied on poor and/or extrapolated ages. Harle (1997) clarified that the palynoflora for MIS5e represented the wettest phase in contrast to the equivalent of MIS5c on land as previous considered by Kershaw et al. (1991) and Kershaw and Nanson (1993). The work also discussed the mode of transport of the pollen and spores retrieved from core E55-6 and argued that the majority of the pollen was transported by wind, but certain taxa had been transported by water such as fern spores, aquatics and myrtaceous shrubs (that have a limited dispersal range, *sic* Harle, 1997). It was also argued that some rainforest taxa such as *Lagarostrobos* and *Phyllocladus* may have been transported from as far as Tasmania, where they are restricted today, but the predominant wind direction would not favour this. Either these taxa occurred in western Victoria or were transported by an oceanic current such as the Flinders Current that travels northward along the western coast of Tasmania (Richardson et al., 2019). Major findings of relevance to the study of core 2697 are: (1) *Callitris* is restricted to MIS 2 and 5d and this parallels our findings on core 2607; (2) *Eucalyptus* counts are highest during the entire MIS 5 (and in particular MIS 5c) and this coincided also with high charcoal counts. In contrast, charcoal counts were also low during MIS 2 as seen in our work in core 2607; and (3) Asteraceae (spiny and spineless) counts fluctuated in discordance with Poaceae pollen, but the trend is opposite to that found in core 2607. During MIS 2, when *Callitris* representation is high (only one sample), *Eucalyptus* is low.

Core SO36-7SL offshore western Tasmania

This core was taken at a water depth of 1,085 m (Fig. 1) and extends as far back as 75 ka BP. A total of 44 samples were analysed and are compared against a $\delta^{18}O$ curve obtained from benthic foraminifera compared against the astronomically tuned time scale established at that time by Martinson et al. (1987). In contrast with the findings from core 2607 and E55-6, rainforest taxa are recognised in all samples, but percentages decreased for MIS stages before the Holocene. The surprise was to find the highest counts of *Lagarostrobos* (commonly known as Huon Pine) during MIS 2. This may have been due to lateral transport conditions at sea since the algae *Botryococcus* and *Pediastrum* were recorded in all samples and these would indicate fluvial transport from inland. *Lagarostrobos* pollen may have been transported to the core site with the Flinders Current since it is most common in SW Tasmania (refer to details discussed for core E55-6, above).

During the warm phases (MIS 5a, 3 and 1) *Eucalyptus* numbers were notably high whereas they were lower during the cold phases (MIS 2 and 4) and it is during those times that grasses numbers peaked. We assume that the alpine/subalpine flora, consisting of herbs and woodland/shrub, would have expanded during the glacial phases. No charcoal counts were reported in the pollen diagram.

The success story of this core his that it permitted a good correlation with pollen records (published at that time) from inland sequences, many of which had gaps for the period spaning 75 ka; this was the same 'achievement' for core E55-6.

Core Fr1/94-GC3

This core was taken on the East Tasman Plateau at a water depth of 2,667 m. With a length of only 4.71m, it is very short for a marine core but the sediment sequence is very condensed, spanning the last 460 ka BP. Only 29 samples cover the last glacial/interglacial cycle, but the advantage of this core record is that it has been possible to compare the last cycle with the 3 previous ones. The core location, on the East Tasman Plateau, is separated from the Tasmanian mainland by a deep trough (see Fig. 1 in De Deckker et al, 2019a) and, consequently, in contrast with the other cores mentioned above, there was no fluvial transport that would have brought pollen to the core site.

The chronology of this core is based on a planktic and benthic $\delta^{18}O$ stratigraphy, so ages are well defined. A variety of proxies was studied from the core, enabling comparison of the pollen record with SST using 3 different techniques (see De Deckker et al., 2019b), as well as estimated seasonal patterns of rainfall and temperature on land.

The salient features interpreted from the pollen record covering the last glacial/interglacial cycle are: (1) alpine taxa are better represented during MIS stages 2 and 4, and late in MIS 3; (2) rainforest taxa were best represented during MIS 5, and to a lesser extent during MIS 3; (3) overall *Eucalyptus* numbers were consistently low during MIS 2, 4 and 6; (4) *Callitris* pollen is absent in that core, implying wetter conditions than on the Australian mainland; and (5) estimates of rainfall on land (obtained from the pollen record) show drying through the record through time and land temperatures reconstructed from the pollen record indicate a temperature rise during MIS 2 which is opposite to the reconstructed sea-surface temperatures. This latter feature is rather puzzling and will need to be revisited, especially since too few samples were used for those reconstructions. Comparing the records from Fr1/94-GC3 and core SO36-7SL, we see almost no alpine taxa in the former during MIS4 while alpine taxa increase in the latter during the same time period. However, there were too few samples to come to a definite answer. In summary, the alpine shrubland and grasses expanded during MIS 2 and 4 (as well as 6 in core GC3).

Core Fr10/95-GC17 offshore NW Western Australia

This core is located on the Exmouth Plateau offshore North West Cape at a water depth of 1093 m. It is located in the subtropics and the salient feature is that, during monsoonal activity, vast amounts of fluvial clays were transported to the ocean. This is reflected in the Holocene sediments by the colour of the upper 88 cm of the sediment which is yellowish brown (10 YR 4/3 on the Munsell Soil Chart). In the lower part of the core, the sediment is coloured olive-grey [7.5Y 5/2]. Obviously, pollen can be transported at sea during the floods, but an aeolian component also must have also prevailed, especially when monsoonal rains would have been absent as shown by the occurrence of airborne clays in the core (Gingele et al., 2001). van der Kaars and De Deckker (2002) and van der Kaars et al. (2006) examined the pollen record of this core spanning a record of 100 ka, with an unfortunate gap recorded from 60 to 46 ka BP. Interpretation of this pollen record varies c considerably from the other core sites discussed above due to the different vegetation types in northwestern Western Australia. De Deckker et al. (2014) re-examined the pollen record for the period spanning the last 34 ka, in conjunction with several other proxies, such as SST reconstruction, monsoonal activity, changes in oceanic productivity and stratification and airborne clays deposited at sea. In that same paper, temperature and rainfall on land were reconstructed from the pollen data based on the work of van der Kaars et al. (2006) and compared with conditions at sea. Importantly, the presence of spores in all the samples in the core inform on the behaviour of the Leeuwin Current (that parallels the coast), bringing pteridophyte spores from as far as Indonesia and/or New Guinea during the second half of the Holocene. Based on the work of van der Kaars and De Deckker (2002), salient vegetational features are that *Callitris* is highest during the LGM (as observed in core 2607 in this present study), with fewer numbers during the middle of the Holocene, part of MIS 3 and commonly occurring during the 95 to 65 ka period. Since the LGM, *Eucalyptus* increased progressively but was never as high as lower down in the core (viz. part of MIS 3 and during the 100 to 65 ka period). Once again, there is good correspondence between the *Eucalyptus* and charcoal (as we note in core 2607).

Noticeable also are the fluctuating levels of Poaceae and Asteraceae/Tubiliflorae: high (~30%) Poaceae and low (~20%) Asteraceae/Tubiliflorae that coincide with predominantly summer rainfall that resulted from monsoonal activity after 13 ka BP. This is in contrast with the LGM and before (De Deckker et al., 2014) when conditions were very different. Alternating levels between those taxa during the second half of the Holocene are likely the result of alternating and

contrasting conditions set by ENSO that was in full force during the last 6,000 years (see Perner et al. (2018) for more information). Lastly, the appearance in the record of mangrove pollen (Rhizophoraceae and *Avicennia*) during the Holocene likely represents stabilization of the coastline, and declines after 6 ka BP as already found by Grindrod et al (1999) for other coastal sites in northern Australia.

Core ODP 820A offshore Queensland adjacent to the Great Barrier Reef

This core was obtained from ODP site 820A at a water depth of 278 m and is adjacent to the humid tropics of northern Australia. It is situated seaward of the Great Barrier Reef on the continental slope, about 40 km from the modern-day coast and about 100 km from Lynch's Crater, a site with an extensive and very detailed pollen record (Kershaw , 1981, 1986; Kershaw et al., 1991, 2007).

The palynofloral record of this core is very different from the others mentioned here as it relates to tropical forests dominated by gymnosperm and angiosperm rainforests. Despite that, and the fact that the $\delta^{18}O$ record of foraminifera for this core is problematic (further discussed below) several distinct trends are noticeable. During the LGM, when sea level had dropped between 124 and 128 m at 20.05 ka BP (Yokoyama et al., 2018), sandy layers are clearly visible in the core (~7.25 m with 60% sand wt%). These resulted from the shallowness of the core site and the same occurs again at ~33 m core depth (Peerdeman and Davies, 1993). These levels correspond to MIS 2 and 6, respectively. In addition, Peerdeman et al. (1993) also mentioned two hiatuses in the upper part of the core (at 8.02 to 12.1 m and 35.55 to 35.8 m) which they argue indicate the absence of MIS 4 and 7. However, further examination of the $\delta^{18}O$ curve displayed in figure 2 in Moss and Kershaw (2000) shows the typical MIS4 shift (OIS4 *sic* in Moss and Kershaw (2000) and it is surprising to see high rainforest gymnosperm counts coinciding with this episode. This further confirms that during MIS4 northern Australia was considerably wetter than was previously estimated, as argued in De Deckker et al. (2020), and also refer to the estimated evapotranspiration potential in central Australia argued by Miller et al. (2016) for this period (discussed in De Deckker et al., 2020). .

At first glance, it appears that the percentage of rainforest gymnosperm taxa were much higher during MIS3 compared to MIS1, and during the LGM sclerophyll herbs made up over 65% of the total palynoflora. As might be expected, glacial conditions affected the vegetation inland. The sandy layer at ~33 m that is representative of MIS 6 had fewer sclerophyll herbs. It could be that reworked sands affected the palynoflora taphonomy resulting from a low sea level stand. Similarly, the peak of *Eucalyptus* preceding the low sea level in Moss and Kershaw (2007; zone 3 in fig. 2) coincides with the highest peak of charcoal recorded in the core. The previous high peak occurs exactly during MIS6 in the sandy layers. Following both charcoal peaks, the mangrove pollen increased rapidly, coinciding each time with a period of marine transgression (refer to discussions in Moss and Kershaw (2013)). Also, aquatic pollen abounds at all levels in the core, not surprising since the core site is so close to the Queensland coast, and an aspect that must be taken into account concerning the origin of the palynoflora. It is possible that the palynoflora recorded at site 820A may have come from the north by ocean currents rather than having been blown offshore from the adjacent Atherton Tablelands where rainforest does grow today, although in reduced areas due to European land clearance (Moss et al., 2017).

The revised chronology of the upper 22 m of the ODP820 record is based on 14 AMS ^{14}C dates on pollen concentrates down to 16 m bsf, and closely aligns the palynomorph events recognised in the core with those identified in terrestrial records in the region (Kershaw et al., 2007). The revised chronology makes it clearer that MIS3 was generally wetter than previously thought and MIS 2 was dry and was followed by climatic amelioration during the Holocene. We note that, at the end of MIS4 as shown in Moss et al. (2013, figs. 3, 4), high percentages of rainforest taxa are present, further confirming that MIS4 was wet in northeastern Australia. Nevertheless, caution is required as humans were likely around and may have affected vegetation through burning.

Supplementary Table 1. Reconstruction of estimated rainfall for the four vegetation type end-members. ANRF = annual rainfall, SUMRF = summer rainfall and WINRF = winter rainfall. See text for further details.

	ANRF	SUMRF	WINRF
EM1	732	100	298
EM2	652	69	263
EM3	725	109	255
EM4	394	78	109

Supplementary Table 2. List of all the ages used to construct the age model for core MD03-2607

	Type of dating	Depth (cm)	pMC		$\delta^{13}C$ (‰ PDB)		^{14}C Age (kBP)		R (^{14}C kyr)	R-corrected ^{14}C Age (kBP)		Calendar Age (ka) *		Comments
			mean	1σ	mean	1σ	mean	1σ		mean	1σ	mean	error	
1	OSL	0										1.070	0.160	
2	^{14}C	5	73.1	1.73	-0.5	0.2	2.600	0.190	0.440	2.160	0.190	1.560	0.670	
3	OSL	24.5										2.380	0.410	
4	^{14}C	25	61.38	1.37	0.0	0.2	4.010	0.180	0.440	3.570	0.180	2.780	0.820	
5	OSL	32.5										3.110	0.670	
6	^{14}C	40	61.12	1.42	0.2	0.2	4.045	0.185	0.440	3.605	0.185	3.860	0.670	
7	OSL	49.5										3.940	0.610	
8	^{14}C	50	53.19	1.2	-0.5	0.2	5.155	0.180	0.440	4.715	0.180	4.720	1.070	
9	OSL	63.5										24.060	2.160	discarded due to turbidity current issue
10	OSL	74.5										5.370	0.610	
11	^{14}C	75	41.48	1.01	-0.1	0.2	7.155	0.195	0.440	6.715	0.195	7.130	1.400	
12	^{14}C	85	39.23	0.96	-0.3	0.2	7.600	0.195	0.440	7.160	0.195	8.410	0.980	
13	^{14}C	95	30.13	0.83	-0.3	0.2	9.720	0.220	0.440	9.280	0.220	9.980	0.960	
14	OSL	99.5										9.980	1.610	
15	^{14}C	100	28.41	0.76	-0.4	0.2	10.190	0.215	0.440	9.750	0.215	10.690	0.960	
16	^{14}C	140	20.71	0.53	-1.1	0.2	12.730	0.205	0.600	12.130	0.205	14.330	0.700	
17	OSL	149.5										15.520	1.300	
18	^{14}C	150	18.53	0.51	-0.7	0.2	13.620	0.220	0.600	13.020	0.220	15.420	0.540	
19	^{14}C	165	15.54	0.45	-0.7	0.2	15.040	0.235	0.600	14.440	0.235	16.500	0.940	
20	OSL	174.5										12.750	1.890	discarded due to turbidity current issue
21	^{14}C	175	12.47	0.38	0.0	0.2	16.810	0.240						discarded
22	^{14}C	175	10.44	0.3	0.0	0.2	18.240	0.230						discarded
23	OSL	199.5										17.600	1.360	
24	^{14}C	200	14.07	0.4	0.3	0.2	15.840	0.225	0.600	15.240	0.225	18.350	0.520	
25	OSL	239.5										19.720	1.390	
26	^{14}C	240	11.43	0.34	0.4	0.2	17.510	0.240	0.600	16.910	0.240	20.230	0.500	
27	^{14}C	260	10.74	0.33	-0.4	0.2	18.010	0.245	0.600	17.410	0.245	20.970	0.480	
28	OSL	279.5										19.580	2.480	
29	^{14}C	280	9.95	0.32	0.0	0.2	18.630	0.260	0.600	18.030	0.260	21.730	0.580	
30	^{14}C	300	9.34	0.25	0.4	0.2	19.130	0.215	0.600	18.530	0.215	22.970	0.930	
31	^{14}C	360	7.02	0.33	0.2	0.2	21.420	0.380	0.700	20.720	0.380	27.360	1.910	
32	^{14}C	430	2.17	0.14	0.0	0.2	30.850	0.500	0.700	30.150	0.500	33.180	2.020	
33	^{14}C	490	?	?	?	?	32.600	0.250	0.700	31.900	0.250	37.340	1.740	
34	^{14}C	528	?	?	?	?	35.215	0.275	0.700	34.515	0.275	40.440	1.430	
35	^{14}C	564	0.53	0.04	0.0		42.140	0.630	0.700	41.440	0.630	44.010	0.980	
36	^{14}C	572	0.53	0.04	0.2	0.2	42.090	0.620	0.700	41.390	0.620	44.760	0.940	
37	^{14}C	588	0.53	0.04	0.1	0.1	42.030	0.620	0.700	41.330	0.620	46.530	0.940	
38	$\delta^{18}O$ tie point	590										47.000		
39	$\delta^{18}O$ tie point	670										50.000		
40	$\delta^{18}O$ tie point	700										54.500		
41	$\delta^{18}O$ tie point	730										56.000		
42	OSL	782-787										54.300	3.700	
43	$\delta^{18}O$ tie point	818										59.000		
44	OSL	844-849										65.400	5.300	
45	OSL	872-878										67.600	4.900	
46	OSL	904-909										70.400	5.100	
47	OSL	912-917										71.700	5.800	
48	$\delta^{18}O$ tie point	914.5										72.000		
49	OSL	1014-1019										80.200	8.000	
50	$\delta^{18}O$ tie point	1030										81.500		
51	$\delta^{18}O$ tie point	1090										93.000		
52	$\delta^{18}O$ tie point	1150										100.000		
53	$\delta^{18}O$ tie point	1210										103.000		
54	$\delta^{18}O$ tie point	1240										110.000		
55	$\delta^{18}O$ tie point	1360										125.000		

Note:

* - cal. ages for ^{14}C samples are shown as modelled mean ages ± 2σ uncertainties

References

Cook, E.J., van der Kaars, S. (2006). Development and testing of transfer functions for generating quantitative climatic estimates from Australian pollen data. *Journal of Quaternary Science, 21*, 723-733. doi.org/10.1002/jqs.1076

De Deckker, P., Arnold, L.J, van der Kaars, S., Bayon, G., Stuut, J-B.W., Perner, K., Lopes dos Santos, R., Uemura, R., Demuro, M. (2019). Marine Isotope Stage 4 in Australasia: a full glacial culminating 65,000 years ago – global

connections and implications for human dispersal. *Quaternary Science Reviews, 204*, 187-207.doi.org/10.1016/j.quascirev.2018.11.017.

De Deckker, P., Barrows, T.T., Rogers, J. (2014). Land–sea correlations in the Australian region: post-glacial onset of the monsoon in northwestern Western Australia. *Quaternary Science Reviews, 105*, 181-194. doi.org/10.1016/j.quascirev.2014.09.030.

De Deckker, P., Barrows, T.T., Stuut, J.-N., van der Kaars, S., Ayress, M.A., Rogers, J., Chaproniere, G.(2019b). Land-sea correlations in the Australian region: 460k years of changes recorded in a deep-sea core offshore Tasmania. Part 2: the marine compared with the terrestrial record. *Australian Journal of Earth Sciences*, 66, 17-35. doi.org/10.1080/08120099.2018.1495101.

De Deckker, P., Moros, M., Perner, K., Blanz, T., Wacker, L., Schneider, R., Barrows, T.T., O'loingsigh, T. Jansen, E. (2020). Climatic evolution in the Australian region over the last 94 ka - spanning human occupancy -, and unveiling the Last Glacial Maximum. *Quaternary Science Reviews* 106593. 10.1016/j.quascirev.2020.106593

De Deckker, P., van der Kaars, S., Macphail. M., Hope, G. (2019a). Land-sea correlations in the Australian region: 460k years of changes recorded in a deep-sea core offshore Tasmania. Part 1: the pollen record. *Australian Journal of Earth Sciences, 66,* 1-15. doi.org/10.1080/08120099.2018.1495100.

Dietze, E., Dietze, M. (2019). Grain-size distribution unmixing using the R package EMMAge. *E&G Quaternary Science Journal, 68,* 29–46. doi.org/10.5194/egqsj-68-29-2019.

Dietze, M., Dietze, E. (2016). EMMAgeo: End-Member Modelling of Grain-Size Data, available at: https://cran.r-project.org/web/packages/EMMAgeo/

Gingele, F.X., De Deckker, P., Hillenbrand, C.-D. (2001). Late Quaternary fluctuations of the Leeuwin Current and palaeoclimates on the adjacent land masses e clay mineral evidence. *Australian Journal of Earth Science, 48*, 867-874. doi.org/10.1046/j.1440-0952.2001.00905.x

Grimm, E.C. (1987). CONISS: A fortran 77 program for stratigraphically constrained cluster analysis by the method of incremental sum of squares. *Computer Geoscience,* **13**, 13-35. doi.org/10.1016/0098-3004(87)90022-7.

Harle, K.J. (1997). Late Quaternary vegetation and climate change in southeastern Australia: Palynological evidence from marine core E55-6. *Palaeogeography, Palaeoclimatology, Palaeoecology, 131*, 465–483. doi.org/10.1016/S0031-0182(97)00016-3.

Hill, P., De Deckker, P. (2004). AUSCAN Seafloor Mapping and Geological Sampling Survey on the Australian Southern Margin by RV *Marion Dufresne* in 2003. *Geoscience Australia Record, 2004/04*, 136pp.

Hogg, A.G., and 14 other authors. (2020). SHCal20 Southern Hemisphere calibration, 0– 55,000 years cal BP. Radiocarbon doi:10.1017/RDC.2020.59.

Kershaw, A.P. (1981). Climatic change and Aboriginal burning in north-east Australia during the last two glacial/interglacial cycles. *Nature, 322*, 47-49.

Kershaw, A.P. (1986). Pleistocene vegetation of the humid tropics of northeastern Queensland, Australia. *Palaeogeography Palaeoclimatology Palaeoecology, 109*, 399-412. doi.org/10.1016/0031-0182(94)90188-0.

Kershaw, A.P., Baird, J.G., D'Costa, D.M., Edney, P.A., Peterson, J.,A., Strickland, K.M. (1991). A comparison of long Quaternary records from the Atherton and Western Plains volcanic sequences. *Geological Society of Australia, Special Publication,* 18, 288-301.

Kershaw, A.P., Bretherton, S.C., van der Kaars, S. (2007). A complete pollen record of the last 230 ka from Lynch's Crater, north-east Australia. *Palaeogeography, Palaeoclimatology, Palaeoecology 251,* 23-45. doi.org/10.1016/j.palaeo.2007.02.015.

Kershaw, A.P., McKenzie, G.M., Porch, N., Roberts, R.G., Brown, J., Heijnis, H., Orr, M.L., Jacobsen, G., Newall, P.R. (2007). A high-resolution record of vegetation and climate through the last glacial cycles from Caledonia Fen, southeastern highlands of Australia. *Journal of Quaternary Science, 22*, 481-500. doi.org/10.1002/jqs.1127.

Kershaw, A.P., Nanson, G.C. (1993). The last full glacial cycle in the Australian region. *Global and Planetary Change, 7,* 1-9. doi.org/10.1016/0921-8181(93)90036-N

Lisiecki, L.E., Stern, J.V. (2016). Regional and global benthic $\delta^{18}O$ stacks for the last glacial cycle. *Paleoceanography, 31,* 1368-1394. https://doi.org/10.1002/2016PA003002.

Lopes dos Santos, R.A., Wilkins, D., De Deckker, P., Schouten, S. (2012). Late Quaternary productivity changes from offshore Southeastern Australia: a biomarker approach. *Palaeogeogeography, Palaeoclimatology, Palaeoecology, 363-364,* 48-56. doi.org/10.1016/j.palaeo.2012.08.013**.**

Lopes dos Santos, R., De Deckker, P., Hopmans, E.C., Magee, J.W., Mets, A., Sinninghe, J.S., Schouten, S. (2013a). Abrupt vegetation change after the Late Quaternary megafaunal extinction in southeastern Australia. *Nature Geoscience,* doi.org/10.1038/NGEO1856.

Lopes dos Santos, R., Spooner, M. I., Barrows, T.T., De Deckker, P., Sinninghe, J.S., Schouten, S. (2013b). Comparison of organic ($U^{K'}_{37}$, TEX^{H}_{86}, LDI) and faunal proxies (foraminiferal assemblages) for reconstruction of late Quaternary sea surface temperature variability from offshore southeastern Australia. *Paleoceanography, 28,* 1–11, doi:10.1002/palo.20035**.**

Martinson, D.G., Pisias, N.G., Hays J.D., Imbrie, J., Moore, T.C., Shackleton, N.J. (1987). Age dating and the orbital theory of the ice ages: development of a high-resolution 0-300,000-year chronostratigraphy. *Quaternary Research, 27,* 1-29. doi.org/10.1016/0033-5894(87)90046-9.

Miller, G.H., Fogel, M.L., Magee, J.W., Gagan, M.K. (2016). Disentangling the impacts of climate and human colonization on the flora and fauna of the Australian arid zone over the past 100 ka using stable isotopes in avian eggshell. *Quaternary Science Reviews, 151,* 27-57. doi.org/10.1016/j.quascirev.2016.08.009.

Moss, P.T., Dunbar, G.B., Thomas, Z., Turney, C., Kershaw, A.P. (2013). A 60000-year record of environmental change for the Wet Tropics of north-eastern Australia based on the ODP 820 marine core. *Journal of Quaternary Science* 32, 704-716. doi.org/10.1002/jqs.2977**.**

Moss, P.T., Kershaw, A.P. (2000). The last glacial cycle from the humid tropics of northeastern Australia: comparison of a terrestrial and a marine record. *Palaeogeography Palaeoclimatology Palaeoecology, 155,* 155–176.

Moss, P.T., Kershaw, A.P. (2007). A late Quaternary marine palynological record (Oxygen isotope stages 1-7) for the Humid Tropics of northeastern Australia based on ODP Site 820). *Palaeogeography, Palaeoclimatology, Palaeoecology,. 251*, 4-22. doi.org/10.1016/S0031-0182(99)00099-1.

Peerdeman, F.M., Davies, P.J. (1993). Sedimentological response of an outer-shelf, upper-slope sequence to rapid changes in Pleistocene eustatic sea level: Hole 820a, northeastern Australian margin. *Proceedings of the Ocean Drilling Program, Scientific Results, 133*, 303-313. doi.org/10.2973/odp.proc.sr.133.236.1993.

Peerdeman, F.M., Davies, P.J, Chivas, A.R. The stable oxygen isotope signal in shallow-water, upper-slope sediments off the Great Barrier Reef (Hole 820A). *Proceedings of the Ocean Drilling Program, Scientific Results, 133*, 163-172. doi.org/10.2973/odp.proc.sr.133.288.1993.

Perner, K., Moros, M., De Deckker, P., Blanz, T., Wacker, L., Telford, R., Siegel, H., Schneider, R., Jansen, E. (2018). Heat export from the tropics drives mid to late Holocene palaeoceanographic changes offshore southern Australia. *Quaternary Science Reviews 180,* 96-110. doi.org/10.1016/j.quascirev.2017.11.033.

R Core Team (2020). R: A language and environment for statistical computing. R Foundation for Statistical Computing, Vienna, Austria. URL https://www.R-project.org/

Richardson , L.E., Middleton, J.F., Kyser, T.K., James, N.P., Opdyke, B.N. (2019). Shallow water masses and their connectivity along the southern Australian continental margin. *Deep-Sea Research Part I,* doi.org/10.1016/j.dsr.2019.103083.

van der Kaars, S., De Deckker, P. (2002). A Late Quaternary pollen record from deep-sea core Fr10/95-GC17 offshore Cape Range Peninsula, northwestern Western Australia. *Reviews in Palaeobototany and Palynolology,* 120, 17-39. doi.org/10.1016/S0034-6667(02)00075-1.

van der Kaars, S., De Deckker, P., Gingele, F.X. (2006). A 100,000 year record of annual and seasonal rainfall and temperature for northwestern Australia based on a marine pollen record. *Journal of Quaternary Research, 21,* 879-889. doi.org/10.1002/jqs.1010.

Yokoyama, Y., et al. (2018). Rapid glaciation and a two-step sea level plunge into the Last Glacial Maximum. *Nature* doi.org/10.1038/s41586-018-0335-4. Doi.org/ 10.1038/s41586-018-0335-4.